arXiv:1106.4376v1 [nucl-th] 22 Jun 2011

Low energy $\omega(\rightarrow \pi^0\gamma)$ meson photoproduction in the Nucleus

Swapan Das [1]
Nuclear Physics Division, Bhabha Atomic Research Centre
Mumbai-400085, India

Abstract

The $\pi^0\gamma$ invariant mass distribution spectra in the $(\gamma, \pi^0\gamma)$ reaction were measured by TAPS/ELSA collaboration to look for the hadron parameters of the ω meson in Nb nucleus. We study the mechanism for this reaction, where we consider that the elementary reaction in Nb nucleus proceeds as $\gamma N \rightarrow \omega N$; $\omega \rightarrow \pi^0\gamma$. The ω meson photoproduction amplitude for this reaction is extracted from the measured four momentum transfer distribution in the $\gamma p \rightarrow \omega p$ reaction. The propagation of the ω meson and the distorted wave function for the π^0 meson in the final state are described by the eikonal form. The ω and π^0 mesons nucleus optical potentials, appearing in the ω meson propagator and π^0 meson distorted wave function respectively, are estimated using the "$t\varrho$" approximation. The effects of pair correlation and color transparency are also studied. The calculated results do not show medium modification for the ω meson produced in the nucleus for its momentum greater than 200 MeV. It occurs since the ω meson dominantly decays outside the nucleus. The dependence of the cross section on the final state interaction is also investigated. The broadening of the ω meson mass distribution spectra is shown to occur due to the large resolution width associated with the detector used in the experiment.

Keywords: ω meson photoproduction, $\pi^0\gamma$ invariant mass distribution, meson nucleus interactions

PACS number(s): 25.20.Lj, 13.75.Lb

1 Introduction

The study for the properties of vector meson in the nuclear medium is a topic of intense interest in the nuclear physics. This topic has been pursued vigorously in recent years to determine quantitatively the mass and width of the vector meson in the nucleus. Various model calculations relate the in-medium properties of vector meson with the chiral symmetry in QCD. The restoration of this symmetry in the nuclear medium predicts the reduction of vector meson mass which could be drastic in the hot and/or dense nuclear medium [1]. Using the scaling property in QCD, Brow and Rho [2] have shown that the

[1]email: swapand@barc.gov.in

vector meson mass should drop in the nuclear medium. Other model calculations, such as QCD sum rule calculations due to Hatsuda et al. [3], VMD model calculations due to Asakawa et al. [4], and the quark meson coupling model calculation due to Saito et al. [5], corroborate this finding. On the other hand, the vector meson mass shift (upward) and width broadening in the hot and dense nuclear matter are also reported [6].

Large medium modification of the ρ meson was indicated first in the enhanced dilepton yield (between 300 and 700 MeV) in CERES and HELIOS ultra-relativistic heavy ion collision data taken sometime around 1995 in CERN-SPS [7]. The quantitative estimation of this modification could not be made in that time because of the poor statistics and resolution of the data. Theoretically, these data have been found compatible with both scenarios: (i) the dropping of ρ meson mass [8], and (ii) the many body interaction of ρ meson with other hadrons in the nuclear medium [9]. Almost after a decade, the STAR experiment at RHIC BNL [10] found the decrease in ρ meson mass $\sim$ 70 MeV in the analysis of the $\pi^+\pi^-$ production data from the peripheral Au+Au collisions. However, the upgraded CERES experiment [11] as well as the dimuon measurements (in the In-In collision) in the NA60 experiment at CERN [12] reported considerable broadening in the ρ meson mass distribution spectrum, but essentially no shift in mass.

The interpretation of the ultra-relativistic heavy-ion collision data is very complicated because this reaction occurs far from the equilibrium state whereas the calculations for the hadronic parameters are done at normal nuclear density and zero temperature (equilibrium state). Therefore, it is more accountable to search the in-medium properties of vector meson in the normal nucleus. In fact, the modification of the vector meson is predicted large enough to observe it in the nuclear reaction with pion and photon beams [13]. The chiral symmetry is also shown to restore partially in the normal nucleus (specifically, inside a heavy nucleus [14]). To be added, the scaling hypothesis [2] and QCD sum rule calculation [3] envisage the reduction ($\sim 15-20\%$) of vector meson mass in a nucleus. There also exist many body calculations which show the drop of mass and increase in width for the vector meson in the normal nucleus [13, 15]. Beside these, only width broadening [16, 17], upward mass-shift [18, 19] and appearance of additional peaks [17, 19, 20] for the vector meson in the nuclear medium are predicted by various model calculations.

The modification of the vector meson in the normal nucleus has been reported by various measurements. The KEK-PS E325 collaboration at KEK [21] found the enhancement in the e^+e^- yield in the p+A reaction at 12 GeV. This enhancement is well understood due to the reduction of the vector meson mass in the nucleus. The sub-threshold ρ meson production experiment on the ^{3}He$(\gamma,\pi^+\pi^-)$X reaction, done by the TAGX collaboration [22], reported large decrease in the ρ meson mass. The ρ meson polarization distribution, measured by this collaboration [23], corroborates this finding. The recent results, published from Jefferson Laboratory, show the broadening of the ρ meson width in the

photonuclear reaction [24]. The mass shift of the ρ meson found in this experiment is insignificant.

Recent past, the CBELSA/TAPS collaboration measured the $\pi^0\gamma$ invariant mass distribution spectrum to look for the medium modification of the ω meson in Nb nucleus [25]. This experiment was done at the electron stretcher accelerator (ELSA) in Bonn using the tagged γ beam of energy spread $0.64 - 2.53$ GeV. The ω meson was detected through its decay $\omega \to \pi^0\gamma$. To minimize the pionic distortion on the ω meson signal, the data were taken for the π^0 meson kinetic energy T_{π^0} larger than 150 MeV. The measured spectrum for the lower ω meson momentum k_ω bin (i.e., $200 < k_\omega(\mathrm{MeV/c}) < 400$) shows distinct ω meson mass modification at ~ 730 MeV, which gradually vanishes with the increase in the ω meson momentum. However, this claim is no more valid [26] as the reanalysis of the data could not reproduced the spectral shape reported in Ref. [25]. The measured distributions show broad width (~ 55 MeV) comparable to the resolution width of the detecting system used in the experimental set-up. In fact, this width is about 6.5 times larger than the free space decay width of the ω meson ($\Gamma_\omega = 8.43$ MeV [27]). Therefore, the width of the ω meson in a nucleus Γ^*_ω can be detected in this set-up if it is enhanced more than 55 MeV. The present status of this topic is summarized in the recent review articles [28].

We study microscopically the mechanism for the $(\gamma, \pi^0\gamma)$ reaction on a nucleus, and compare our results with the data taken by the CBELSA/TAPS collaboration. In the energy region of this reaction, the elementary reaction occurring in the nucleus can be visualized as $\gamma N \to VN$; $V \to \pi^0\gamma$, where V stands for the low energy vector mesons, i.e., $\rho^0,\ \omega,\ \phi$ mesons. The qualitative analysis presented in Ref. [29] shows that the $\pi^0\gamma$ event in the elementary reaction arises distinctly due to the decay of the ω meson produced in the intermediate state. The contributions to this event from the ρ^0 and ϕ mesons are found negligible. Therefore, we consider that the $(\gamma, \pi^0\gamma)$ reaction on the nucleus proceeds through the formation of ω meson in the intermediate state. The production of this meson is described by the $\gamma N \to \omega N$ reaction amplitude $f_{\gamma N \to \omega N}$, and its propagation is presented by the eikonal form. The ω meson interaction with the nucleus (which appears in its propagator) is described by the corresponding optical potential. The decay of ω meson to π^0 and γ bosons is governed by the $\omega\pi\gamma$ Lagrangian. The π^0 meson scattering state is generated by using the π^0 meson nucleus optical potential.

2 Formalism

The generalized optical potential or self-energy for the photoproduction of ω meson in a nucleus [29, 30] is given by

$$\Pi_{\gamma A\to\omega A}(\mathbf{r}) = -4\pi\left[1+\frac{E_\omega}{E_N}\right] f_{\gamma N\to\omega N}(0)\varrho(\mathbf{r}), \tag{1}$$

where $\varrho(\mathbf{r})$ represents the spatial density distribution of the nucleus.

The factor $f_{\gamma N\to\omega N}(0)$ in Eq. (1) is the forward reaction amplitude for the elementary $\gamma N\to\omega N$ process. It is related to the four momentum q^2 transfer distribution $d\sigma(\gamma N\to\omega N)/dq^2$ [31]:

$$\frac{d\sigma}{dq^2}(\gamma N\to\omega N; q^2=0) = \frac{\pi}{k_\gamma^2}|f_{\gamma N\to\omega N}(0)|^2. \tag{2}$$

The forward $d\sigma(\gamma p\to\omega p)/dq^2$ is used to be obtained by extrapolating the measured value of $d\sigma(\gamma p\to\omega p; q^2)/dq^2$ at $q^2=0$. In fact, the energy dependent values for it are reported in Refs. [31, 32] for $E_\gamma \geq 1.6$ GeV. At lower energies, i.e., $E_\gamma \leq 2.6$ GeV, the four-momentum transfer distributions $d\sigma(\gamma p\to\omega p)/dq^2$ were measured with SAPHIR detector at electron stretcher ring (ELSA), Bonn [33]. We extract the energy dependent $|f_{\gamma p\to\omega p}(0)|^2$ from the measured $d\sigma(\gamma p\to\omega p)/dq^2$, and use them in our calculation.

The omega meson, produced in the nucleus, propagates certain distance before it decays into π^0 and γ bosons. The propagation of the ω meson from its production point $\mathbf{r}$ to its decay point $\mathbf{r}'$ can be expressed as $(-g^\mu_{\mu'}+\frac{1}{m^2}k^\mu_\omega k_{\omega,\mu'})G_\omega(m;\mathbf{r}'-\mathbf{r})$ [34]. We represent the scalar part of the ω meson propagator $G_\omega(m;\mathbf{r}'-\mathbf{r})$ by the eikonal form [35, 36], i.e.,

$$G_\omega(m;\mathbf{r}'-\mathbf{r}) = \delta(\mathbf{b}'-\mathbf{b})\Theta(z'-z)e^{i\mathbf{k}_\omega.(\mathbf{r}'-\mathbf{r})}D_{\mathbf{k}_\omega}(m;\mathbf{b},z',z). \tag{3}$$

The factor $D_{\mathbf{k}_\omega}(m;\mathbf{b},z',z)$ appearing in this equation describes the nuclear medium effect on the properties of ω meson. The form for it is

$$D_{\mathbf{k}_\omega}(m;\mathbf{b},z',z) = -\frac{i}{2k_{\omega\|}}exp\left[\frac{i}{2k_{\omega\|}}\int_z^{z'}dz''\{\tilde{G}_{0\omega}^{-1}(m)-2E_\omega V_{O\omega}(\mathbf{b},z'')\}\right], \tag{4}$$

where k_ω is the momentum of the ω meson. $V_{O\omega}(\mathbf{b},z'')$ represents the ω meson nucleus optical potential which arises due to the interaction of this meson with the particles present in the nucleus. In fact, this potential modifies the hadronic parameters of the ω meson during its passage through the nucleus. $\tilde{G}_{0\omega}(m)$ denotes the ω meson (on-shell) propagator in free space: $\tilde{G}_{0\omega}^{-1}(m) = m^2-m_\omega^2+im_\omega\Gamma_\omega(m)$. Here, m_ω and $\Gamma_\omega(m)$ represent the resonant mass and total decay width for the ω meson, elaborated in Ref. [29].

The $\pi^0\gamma$ in the final state originates due to the decay of ω meson, i.e., $\omega \to \pi^0\gamma$. The Lagrangian density $\mathcal{L}_{\omega\pi\gamma}$ describing this decay channel [29, 37] is given by

$$\mathcal{L}_{\omega\pi\gamma} = -\frac{f_{\omega\pi\gamma}}{m_\pi}\epsilon_{\mu\nu\rho\sigma}\partial^\mu A^\nu \pi \partial^\rho \omega^\sigma, \tag{5}$$

where $f_{\omega\pi\gamma}(= 0.095)$ denotes the $\omega\pi\gamma$ coupling constant. A^ν represents the photon field.

The wave function for photon is described by the plane wave. The distorted wave function $\chi^{(-)}(\mathbf{k_{\pi^0}}, \mathbf{r'})$ for the π^0 meson in the final state is represented by the eikonal form [35, 38]:

$$\chi^{(-)*}(\mathbf{k_{\pi^0}}, \mathbf{r'}) = e^{-i\mathbf{k_{\pi^0}}.\mathbf{r'}} D^{(-)*}_{\mathbf{k_{\pi^0}}}(\mathbf{b}, z'). \tag{6}$$

The factor $D^{(-)*}_{\mathbf{k_{\pi^0}}}(\mathbf{b}, z')$ in this equation describes the pionic distortion. The form for it is

$$D^{(-)*}_{\mathbf{k_{\pi^0}}}(\mathbf{b}, z') = exp\left[-\frac{i}{v_{\pi^0\parallel}}\int_{z'}^{\infty} dz_1 V_{O\pi^0}(\mathbf{b}, z_1)\right], \tag{7}$$

where v_{π^0} is the velocity of pion. $V_{O\pi^0}(\mathbf{b}, z_1)$ denotes the optical potential for the pion nucleus scattering in the final state.

The differential cross section for the ω meson mass m (i.e., the $\pi^0\gamma$ invariant mass) distribution can be written as

$$\frac{d\sigma(m, E_\gamma)}{dm} = \int d\Omega_\omega K_F \Gamma_{\omega\to\pi^0\gamma'}(m)|F(\mathbf{k}_\gamma, \mathbf{k}_\omega)|^2, \tag{8}$$

where K_F is the kinematical factor of the reaction. It is given by $K_F = \frac{1}{(2\pi)^3}\frac{k_\omega}{k_\gamma}m^2$; with $\mathbf{k}_\omega = \mathbf{k}_{\pi^0} + \mathbf{k}_{\gamma'}$. The prime represents the quantity in the final state.

$\Gamma_{\omega\to\pi^0\gamma}(m)$ in above equation denotes the width for the ω meson of mass m decaying at rest into $\pi^0\gamma$ channel. $\Gamma_{\omega\to\pi^0\gamma}(m)$ is evaluated [29] using the Lagrangian density $\mathcal{L}_{\omega\pi\gamma}$ given in Eq. (5):

$$\Gamma_{\omega\to\pi^0\gamma}(m) = \Gamma_{\omega\to\pi^0\gamma}(m_\omega)\left[\frac{k(m)}{k(m_\omega)}\right]^3, \tag{9}$$

with $\Gamma_{\omega\to\pi^0\gamma}(m_\omega = 782\text{ MeV}) \approx 0.72$ MeV. $k(m)$ is the momentum of pion in the $\pi^0\gamma$ cm system.

The factor $F(\mathbf{k}_\gamma, \mathbf{k}_\omega)$ in Eq. (8) describes the production of ω meson in the nucleus. In addition, it also carries the information about the ω meson propagation inside as well as outside the nucleus. The expression for it is

$$F(\mathbf{k}_\gamma, \mathbf{k}_\omega) = \int d\mathbf{r}\Pi_{\gamma A\to\omega A}(\mathbf{r}) e^{i(\mathbf{k}_\gamma - \mathbf{k}_\omega).\mathbf{r}} D(\mathbf{k}_\omega; \mathbf{b}, z), \tag{10}$$

where $D(\mathbf{k}_\omega; \mathbf{b}, z)$ is given by

$$D(\mathbf{k}_\omega; \mathbf{b}, z) = \int_z^\infty dz' D^{(-)*}_{\mathbf{k}_{\pi^0}}(\mathbf{b}, z') D_{\mathbf{k}_\omega}(\mathbf{b}, z', z). \tag{11}$$

All quantities appearing in this equation are already defined. The ω meson decay probabilities inside and outside the nucleus can be addressed by splitting $D(\mathbf{k}_\omega; \mathbf{b}, z)$ in Eq. (11) into two parts:

$$D(\mathbf{k}_\omega; \mathbf{b}, z) = D_{in}(\mathbf{k}_\omega; \mathbf{b}, z) + D_{out}(\mathbf{k}_\omega; \mathbf{b}, z), \tag{12}$$

where $D_{in}(\mathbf{k}_\omega; \mathbf{b}, z)$ and $D_{out}(\mathbf{k}_\omega; \mathbf{b}, z)$ describe the ω meson decay inside and outside the nucleus respectively. Using Eq. (11), they can be written as

$$D_{in}(\mathbf{k}_\omega; \mathbf{b}, z) = \int_z^Z dz' D^{(-)*}_{\mathbf{k}_{\pi^0}}(\mathbf{b}, z') D_{\mathbf{k}_\omega}(\mathbf{b}, z', z), \tag{13}$$

$$D_{out}(\mathbf{k}_\omega; \mathbf{b}, z) = \int_Z^\infty dz' D^{(-)*}_{\mathbf{k}_{\pi^0}}(\mathbf{b}, z') D_{\mathbf{k}_\omega}(\mathbf{b}, z', z), \tag{14}$$

with $Z = \sqrt{R^2 - b^2}$. R is the extension of the nucleus. In fact, $D_{out}(\mathbf{k}_\omega; \mathbf{b}, z)$ in the above equation can be simplified to $\tilde{G}_{0\omega}(m) exp[\frac{i}{2k_\omega} \tilde{G}^{-1}_{0\omega}(m)(Z - z)]$.

The Eq. (8) illustrates the differential cross section for the ω meson mass distribution due to fixed γ beam energy E_γ. But, as we mentioned earlier, the CBELSA/TAPS collaboration [25] used tagged photon beam of definite energy range in their measurement. Therefore, we modulate the cross section in Eq. (8) with the beam profile function $W(E_\gamma)$ [39], i.e.,

$$\frac{d\sigma(m)}{dm} = \int_{E_\gamma^{mn}}^{E_\gamma^{mx}} dE_\gamma W(E_\gamma) \frac{d\sigma(m, E_\gamma)}{dm}. \tag{15}$$

E_γ^{mn} and E_γ^{mx} are equal to 0.64 GeV and 2.53 GeV respectively, as provided in Ref. [25]. The profile function $W(E_\gamma)$ for the γ beam (originating due to the bremsstrahlung radiation of electron impinging on the Pb target [25]) varies as $W(E_\gamma) \propto \frac{1}{E_\gamma}$ [39].

3 Results and Discussions

We calculate the ω meson mass m (i.e., the $\pi^0\gamma$ invariant mass) distribution spectra in the $(\gamma, \omega \to \pi^0\gamma)$ reaction on ^{93}Nb nucleus. The ω meson, as mentioned earlier, is detected for pion (arising due to $\omega \to \pi^0\gamma$) kinetic energy T_{π^0} greater than 150 MeV. We impose this condition in our calculation, i.e., all results presented in this manuscript are calculated for $T_{\pi^0} > 150$ MeV.

The meson nucleus optical potentials, i.e., $V_{O\omega}$ in Eq. (4) and $V_{O\pi^0}$ in Eq (7), are estimated using the "$t\varrho$" approximation [35]:

$$V_{OM}(\mathbf{r}) = -\frac{v_M}{2}[i + \alpha_{MN}]\sigma_t^{MN} \varrho(\mathbf{r}). \tag{16}$$

The symbol M in this equation stands for a meson (i.e., either ω meson or π^0 meson), and N denotes a nucleon. v_M is the velocity of the meson M. α_{MN} represents the ratio of the real to imaginary part of the meson nucleon scattering amplitude f_{MN}, and σ_t^{MN} is the corresponding total cross section. Since the ω meson is a neutral unstable particle, $\alpha_{\omega N}$ and $\sigma_t^{\omega N}$ can't be obtained directly from measurements. Lutz et al., [40] (using couple channel calculation) have estimated the energy dependent $f_{\omega N}$ in the low energy region, i.e., $1.4 \leq \sqrt{s}(\mathrm{GeV}) \leq 1.8$. Their calculations are well constrained by the elementary ω meson production data in the threshold region. At higher energy, the imaginary part of $f_{\omega N}$ is extracted from the elementary ω meson photoproduction data using vector meson dominance model [37, 41]. Sibirtsev et al. [41], using additive quark model and Regge theory, have evaluated $f_{\omega N}$ for a wide range of energy. According to them $\alpha_{\omega N}$ can be written as $\alpha_{\omega N} = \frac{0.173(s/s_0)^{\epsilon} - 2.726(s/s_0)^{-\eta}}{1.359(s/s_0)^{\epsilon} + 3.164(s/s_0)^{-\eta}}$, with $s_0 = 1$ GeV^2, $\epsilon = 0.08$ and $\eta = 0.45$ [41]. For $V_{O\pi^0}(\mathbf{r})$ also, the energy dependent $\alpha_{\pi^0 N}$ and $\sigma_t^{\pi^0 N}$ can't be measured directly. Therefore, we have worked out the π^0 meson nucleon scattering amplitude $f_{\pi^0 N}$ using isospin algebra: $f_{\pi^0 N} = \frac{1}{2}[f_{\pi^+ N} + f_{\pi^- N}]$. The energy dependent measured values for the $\pi^{\pm} N$ scattering parameters, i.e., $\alpha_{\pi^{\pm} N}$ and $\sigma_t^{\pi^{\pm} N}$, are available in Ref. [42].

The nuclear density distribution $\varrho(\mathbf{r})$, required to evaluate Eqs. (1) and (16), is approximated by the nuclear charge density distribution. The form of $\varrho(\mathbf{r})$ for ^{93}Nb nucleus, as obtained from the electron scattering data, is given by

$$\varrho(\mathbf{r}) = \varrho_0 \frac{1}{1 + exp(\frac{r-c}{z})}; \tag{17}$$

with c=4.87 fm, z=0.573 fm [43]. It is normalized to the mass number of the nucleus. The pair correlation (PC) in $\varrho(\mathbf{r})$ can be incorporated by the following replacement [30]:

$$\varrho(\mathbf{r}) \rightarrow \varrho(\mathbf{r}) \left[1 + \frac{1}{2} \sigma_t^{MN} \varrho(\mathbf{r}) l_c \left\{ \frac{\varrho(\mathbf{r})}{\varrho(0)} \right\}^{1/3} \right], \tag{18}$$

where the correlation length l_c is equal to 0.3 fm [30]. We include α_{MN} in the above equation by the trivial substitution $\sigma_t^{MN} \rightarrow (1 - i\alpha_{MN})\sigma_t^{MN}$ [38].

The onset of color transparency (CT) has been reported in many nuclear pion production reactions at intermediate energies [44, 45]. The color transparency arises due to the reduction of the elementary pion nucleon total cross section over a typical length scale, commonly known as hadron formation length l_h. The standard expression for the effective cross section (which incorporates CT effect in it [45]) is

$$\frac{\sigma_{t,eff}^{\pi^0 N}}{\sigma_t^{\pi^0 N}} = \left[\left\{ \frac{z}{l_h} + \frac{n^2 k_t^2}{Q^2} \left(1 - \frac{z}{l_h} \right) \right\} \theta(l_h - z) + \theta(z - l_h) \right]. \tag{19}$$

The value of n is equal to 2 for a quark-antiquark color singlet system. k_t (=0.35 GeV/c) is the average transverse momentum of a quark inside the hadron. z is the straight path travelled by the pion after its formation. In above equation, $Q^2 = |(k^\mu_\gamma - k^\mu_{\gamma'})^2|$, and $l_h \equiv l_{\pi^0} \simeq 2k_{\pi^0}/(0.7\ \mathrm{GeV}^2)$ [45].

The main purpose of this calculation is to look for the in-medium properties of ω meson in the nucleus. We, therefore, present in Fig. 1 the ω meson mass distribution spectra calculated with and without the ω meson nucleus (i.e., Nb nucleus) interaction for $k_\omega(\mathrm{GeV/c}) = 0.21 - 0.39$. As mentioned earlier, it is the lowest ω meson momentum bin in the measurement where the medium modification was shown to occur [25]. The solid curve in Fig. 1 represents the previous case, i.e., the ω meson nucleus interaction is incorporated in the calculated cross section. The cross section calculated without this interaction is presented by the dot-dot-dashed curve. In both cases, the pion nucleus interaction has been incorporated. This figure distinctly shows the absence of medium modification for the ω meson photoproduced in the Nb nucleus for $0.2 < k_\omega(\mathrm{GeV/c}) < 0.4$.

Since Fig. 1 does not show the medium modification of the ω meson produced in the Nb nucleus, we envisage to compare the ω meson decay probabilities inside and outside the nucleus for the same kinematical condition quoted in Fig. 1, i.e., $0.2 < k_\omega(\mathrm{GeV/c}) < 0.4$. In Fig. 2, we plot the mass distribution spectra for the ω meson decaying inside and outside the Nb nucleus. This figure shows that the ω meson decays dominantly outside the nucleus (dashed curve). The cross section for the ω meson decaying inside the nucleus is presented by the dot-dashed curve. The solid curve in Fig. 2 illustrates that the coherent addition of the amplitudes of the ω meson decaying inside and outside the nucleus enhances the cross section significantly at the peak. For $k_\omega > 0.4$ GeV/c, the ω meson moves faster resulting less interaction with the nucleus. In such case, the cross section for the ω meson decaying outside the nucleus would be relatively larger than that shown in Fig. 2. Therefore, the medium effect on the ω meson in Nb nucleus is hardly possible under this circumstances.

It should be mentioned that the ω meson decays throughout its passage inside as well as outside the nucleus. The decay probability of this meson inside the nucleus would be larger if its effective decay length $L^*_\omega (= v_\omega/\Gamma^*_\omega)$ in the nucleus is less than the dimension of the nucleus. Here, v_ω and Γ^*_ω denote the velocity and the effective width of the ω meson in the nucleus. Since the width of ω meson in the free state (i.e., Γ_ω) is equal to 8.43 MeV, the free space ω meson decay length $L_\omega (= v_\omega/\Gamma_\omega)$ is about 5.8 fm for k_ω equal to 200 MeV/c. This decay length would be much larger for k_ω equal to 400 MeV/c ($L_\omega \sim 10.66$ fm for $k_\omega = 400$ MeV/c). Therefore, L_ω for $k_\omega = 200 - 400$ MeV is significantly larger than the radius of ^{93}Nb nucleus ($R_{rms} \sim 4.3$ fm). The above analysis shows that the ω meson can't decay inside the Nb nucleus unless its width in this nucleus is drastically increased, i.e., $\Gamma^*_\omega >> \Gamma_\omega$.

We present in Fig. 3 the calculated results showing the effect of pionic distortion on the ω meson mass distribution spectrum for $0.2 < k_\omega(\mathrm{GeV/c}) < 0.4$. This figure shows

that the calculated cross section is not sensitive to the pion nucleus interaction. The decay of ω meson ($\rightarrow \pi^0\gamma$) dominantly outside the nucleus (shown in Fig. 2) causes the cross section insensitive to this interaction. The incorporation of color transparency (CT) in the pion nucleus interaction (see Eq. (19)) does not make any change in the calculated spectrum. Therefore, we do not show it. In fact, the cross section, as mentioned above, is not sensitive to the pion nucleus interaction itself. It could be added that CT is a high energy phenomenon, i.e., $Q^2 \geq 1$. Large hadron formation length l_h (which occurs at higher pion momentum) is also needed for the color transparency. Therefore, CT is not expected in the low energy nuclear reaction, as considered in this manuscript.

The sensitivity of the pair correlation (PC) to the calculated cross section is presented in Fig. 4. The solid curve in this figure shows the calculated ω meson mass distribution spectrum where PC is included in the nuclear density distribution (see $\varrho(\mathbf{r})$ in Eqs. (17) and (18)). The dashed curve represents the calculated spectrum without PC incorporated in the nuclear density distribution, i.e., $\varrho(\mathbf{r})$ given in Eq. (17). To be mentioned, PC is included in all other results shown in this manuscript. Fig. 4 shows that the incorporation of PC increases the magnitude of the calculated cross section significantly, i.e., by a factor of ~ 1.46 at the peak.

The broad width appearing in the measured $\pi^0\gamma$ invariant mass distribution spectra can be presumed due to the large resolution width ($\sim$ 55 MeV) in the detecting system used in the experimental set-up [25]. We incorporate this in our formalism by folding a Gaussian function $R(m, m')$ with the differential cross section given in Eq. (15), i.e.,

$$\frac{d\sigma(m)}{dm} = \int dm' R(m, m') \frac{d\sigma(m')}{dm'}. \tag{20}$$

The function $R(m, m')$ in this equation accounts the resolution width for the detector used in the measurement. It is given by

$$R(m, m') = \frac{1}{\sigma\sqrt{2\pi}} e^{-\frac{(m-m')^2}{2\sigma^2}}, \tag{21}$$

where σ is related to the full width at half-maxima of the resolution function $R(m, m')$: FWHM= 2.35σ [46]. The value of FWHM is taken equal to the width of the detector resolution, i.e., 55 MeV as given in Ref. [25]. Fig. 5 shows that the incorporation of the detector resolution function in the calculation reduces the cross section at the peak, and it enhances simultaneously the width of the cross section.

We present in Fig. 6 the calculated results due to Eq. (20) along with the measured $\pi^0\gamma$ invariant mass distribution spectra (histograms, taken from the Ref. [25]) for the ω meson momentum bins: (i) $0.6 < k_\omega(\text{GeV/c}) < 1$ and (ii) $1 < k_\omega(\text{GeV/c}) < 1.4$. The solid curves appearing in this figure denote the calculated spectra for (i) $k_\omega = 0.61 - 0.99$ GeV/c and (ii) $k_\omega = 1.01 - 1.39$ GeV/c. It is noticeable in this figure that the calculated distributions

reproduce the data very well. As mentioned earlier, the CB/TAPS collaboration reported the modification of ω meson mass in the Nb nucleus in the region below 780 MeV for $0.2 < k_\omega(\mathrm{GeV/c}) < 0.4$ and $0.4 < k_\omega(\mathrm{GeV/c}) < 0.6$ [25]. Since this claim is no longer valid [26], we do not compare the calculated results with the data for $k_\omega < 0.6$ GeV/c.

4 Conclusions

We have studied the mechanism for the $(\gamma, \pi^0\gamma)$ reaction on Nb nucleus in the energy region: $0.64 - 2.54$ GeV. The π^0 and γ bosons appearing in coincidence in the final state are shown to originate due to the decay of ω meson produced in the intermediate state. The calculated results show that the properties of ω meson in the nucleus are not modified for the kinematics used in the measurement done at ELSA. It occurs since the ω meson dominantly decays outside the nucleus. This is also the reason for not showing the distortion due to final state interaction, i.e., the π^0 meson nucleus interaction. The incorporation of color transparency in the pion nucleus interaction does not change the cross section for the ω meson mass distribution. The inclusion of pair correlation in the nuclear density distribution increases the magnitude of the cross section. The broad width in the measured distribution is found to arise due to the large resolution width associated with the detector used in the experiment. The calculated results reproduce the measured spectra very well.

5 Acknowledgement

I gratefully acknowledge Dr. L. M. Pant for making me aware about the measurement for the omega meson mass distribution. The communication made with Prof. Dr. E. Oset regarding the beam profile function is very helpful. The discussion with Dr. D. R. Chakrabarty on the detector resolution is highly appreciated.

References

[1] C. M. Ko, V. Koch and G. Li, Annu. Rev. Nucl. Part. Sci. **47**, 505 (1997); W. Cassing and E. L. Bratkovskaya, Phys. Rep. **308**, 65 (1999); R. Rapp and J. Wambach, Adv. Nucl. Phys. **25**, 1 (2000).

[2] G. E. Brown and M. Rho, Phys. Rev. Lett. **66**, 2720 (1991).

[3] T. Hatsuda and S. H. Lee, Phys. Rev. C **46**, R34 (1992).

[4] M. Asakawa, C. M. Ko, P. Levai and X. J. Qiu, Phys. Rev. C **46**, R1159 (1992); M. Asakawa and C. M. Ko, Phys. Rev. C **48**, R526 (1993); M. Asakawa and C. M. Ko, Nucl. Phys. **A560**, 399 (1993).

[5] K. Saito, K. Tsushima and A. W. Thomas, Phys. Rev. C **55**, 2637 (1997).

[6] M. Urban, M. Buballa, R. Rapp, and J. Wambach, Nucl. Phys. A **673**, 357 (2000).

[7] A. Drees, Nucl. Phys. **A610**, 536c (1996); CERES Collaboration, Th. Ullrich, Nucl. Phys. **A610**, 317c (1996); HELIOS-3 Collaboration, M. Masera, Nucl. Phys. **A590**, 93c (1995); NA50 Collaboration, E. Scomparin, Nucl. Phys. **A610**, 331c (1996).

[8] G. Q. Li, C. M. Ko and G. E. Brown, Phys. Rev. Lett. **75**, 4007 (1995); G. Q. Li, C. M. Ko, G. E. Brown and H. Sorge, Nucl. Phys. **A611**, 539 (1996); W. Cassing, W. Ehehalt and C. M. Ko, Phys. Lett. B **363**, 35 (1995); W. Cassing, W. Ehehalt and I. Karlik, Phys. Lett. B **377**, 5 (1996).

[9] G. Chanfray, R. Rapp and J. Wambach, Phys. Rev. Lett. **76**, 368 (1996); R. Rapp, G. Chanfray and J. Wambach, Nucl. Phys. **A617**, 472 (1997); W. Cassing, E. L. Bratkovskaya, R. Rapp and J. Wambach, Phys. Rev. C **57**, 916 (1998); R. Rapp, J. Wambach, Eur. Phys. J **A6**, 415 (1999); T. Renk, R. Schneider and W. Weise, Phys. Rev. C **66**, 014902 (2002).

[10] J. Adams et al., Phys. Rev. Lett. **92**, 092301 (2004).

[11] D. Adamová et al., arXiv:nucl-ex/0611022v3; Phys. Lett. B **666** 425 (2008).

[12] R. Arnaldi et al., Phys. Rev. Lett. **96**, 162302 (2006); Eur. Phys. J. C **49** 235 (2007); S. Damjanovic et al., Nucl. Phys. A **783** 327c (2007).

[13] M. Effenberger, E. L. Bratkovskaya, and U. Mosel, Phys. Rev. C **60**, 044614 (1999); Th. Weidmann, E. L. Bratkovskaya, W. Cassing and U. Mosel, Phys. Rev. C **59**, 919 (1999); M. Effenberger, E. L. Bratkovskaya, W. Cassing and U. Mosel, Phys. Rev. C **60**, 027601 (1999).

[14] M. C. Birse, J. Phys. G: Nucl. Part. Phys. **20** 1537 (1994).

[15] F. Klingl et al., Z. Phys. A **356** 193 (1996); Nucl. Phys. A **650** 299 (1999).

[16] D. Cabrera and M. J. Vicente Vacas, Phys. Rev. C **67**, 045203 (2003); D. Cabrera, L. Roca, E. Oset, H. Toki and M. J. Vicente Vacas, Nucl. Phys. A **733**, 130 (2004); V. K. Magas, L. Roca and E. Oset, Phys. Rev. C **71** 065202 (2005), arXiv:nucl-th/0403067v2.

[17] M. Herrmann, B.L. Friman and W. Nörenberg, Z. Phys. **A343**, 119 (1992); Nucl. Phys. **A560**, 411 (1993).

[18] A. K. Dutt-Mazumder, R. Hoffmann and M. Pospelov, Phys. Rev. C **63** 015204 (2000); S. Zschocke, O.P. Pavlenko and B. Kamper, Phys. Lett. B **562** 57 (2003).

[19] D. Cabrera, E. Oset and M. J. Vicente Vacas, Nucl. Phys. A **705** 90 (2002).

[20] M. Post, S. Leupold and U. Mosel, Nucl. Phys. A **741** 81 (2004).

[21] R. Muto et al., J. Phys. G: Nucl. Part. Phys. **30**, S1023 (2004); M. Nakuri et al., Phys. Rev. Lett. **96**, 092301 (2006); R. Muto et al. (KEK-PS E325 Collaboration), Phys. Rev. Lett. **98**, 042501 (2007).

[22] G. J. Lolos et al., Phys. Rev. Lett. **80**, 241 (1998).

[23] G. M. Huber et al. (TAGX Collaboration), Phys. Rev. C **68**, 065202 (2003).

[24] R. Nasseripour et al. (CLAS Collaboration), Phys. Rev. Lett. **99**, 262302 (2007); M. H. Wood et al. (CLAS Collaboration), Phys. Rev. C **78** 015201 (2008).

[25] CBELSA/TAPS Collaboration, D. Trnka et al., Phys. Rev. Lett. **94**, 192303 (2005).

[26] M. Nanova et al., Phys. Rev. C **82** 035209 (2010), arXiv:1005.5694 [nucl-ex]; Eur. Phys. J. A **47** 16 (2011), arXiv:1008.4520 [nucl-ex]; V. Metag, private communication.

[27] Particle Data Group, Phys. Rev. D **54**, 333 (1996).

[28] S. Leupold, V. Metag and U. Mosel, Int. J. Mod. Phys. E **19**, 147 (2010), arXiv:0907.2388 [nucl-th]; R. S. Hayano and T. Hatsuda, Rev. Mod. Phys. **82**, 2949 (2010), arXiv:0812.1702 [nucl-ex].

[29] Swapan Das, Phys. Rev. C **78**, 045210 (2008).

[30] A. Pautz and G. Shaw, Phys. Rev. C **57** 2648 (1998).

[31] A. Sibirtsev, H.-W. Hammer, U.-G. Meißner and A.W. Thomas, Eur. Phys. J. A **29** 209 (2006).

[32] A. Sibirtsev, K. Tsushima and S. Krewald, Phys. Rev. C **67** 055201 (2003).

[33] J. Barth et al., Eur. Phys. J. A **18**, 117 (2003).

[34] Swapan Das, Pramana **75**, 665 (2010).

[35] Swapan Das, Phys. Rev. C **72**, 064619 (2005).

[36] Ye. S. Golubeva, L. A. Kondratyuk and W. Cassing, Nucl. Phys. A **625**, 832 (1997).

[37] G. I. Lykasov, W. Cassing, A. Sibirtsev, and M. V. Rzjanin, Eur. Phys. J. A **6** 71 (1999).

[38] R. J. Glauber, in Lectures in theoretical physics, edited by W. E. Brittin et al., (Interscience Publishers, New York, 1959) vol. 1, p. 315.

[39] M. Kaskulov, E. Hernandez and E. Oset, arXiv:nuclt-th/0610067; Eur. Phys. J. A **31** 245 (2007).

[40] M. F. M. Lutz, Gy. Wolf and B. Friman, Nucl. Phys. A **706**, 431 (2002).

[41] A. Sibirtsev, Ch. Elster and J. Speth, arXiv:nucl-th/0203044.

[42] Particle Data Group, Phys. Rev. D **54**, 192-195 (1996);
http://pdg.lbl.gov/xsect/contents.html.

[43] C. W. De Jager, H. De. Vries and C. De. Vries, At. Data Nucl. Data Tables, **14**, 479 (1974).

[44] B. Clasie et al., Phys. Rev. Lett. **99** 242502 (2007).

[45] W. Cosyn, M. C. Martínez, J. Ryckebusch and B. Van Overmeire, Phys. Rev. C **74** 062201(R) (2006); A. Larson, G. A. Miller and M. Strikman, Phys. Rev. C **74** 018201 (2006); G. R. Farrar, H. Liu, L. L. Frankfurt and M. I. Strikman, Phys. Rev. Lett. **61** 686 (1988).

[46] G. F. Knoll, Radiation Detection and Measurement (John Wiley & Sons, New York, Singapore, 1989), p. 116.

Figure Captions

1. (color online). The calculated ω meson (photoproduced in ^{93}Nb nucleus) mass distribution spectra with (solid curve) and without (dot-dot-dashed curve) the ω meson nucleus interaction for $k_\omega(\mathrm{GeV/c}) = 0.21 - 0.39$. The π^0 meson nucleus interaction is incorporated in both cases.

2. (color online). The calculated mass distribution spectra for the ω meson decaying inside as well as outside ^{93}Nb nucleus. The dot-dashed curve represents the cross section for the ω meson decaying inside the nucleus, whereas the dashed curve corresponds to its decay outside the nucleus. The coherent addition of them is shown by the solid curve.

3. (color online). The effect of pionic distortion on the ω meson mass distribution spectrum for $k_\omega(\mathrm{GeV/c}) = 0.21 - 0.39$. The dotted curve represents the calculated spectrum where the plane wave for π^0 meson is considered in the calculation. The incorporation of the pionic distortion, as shown by the solid curve, hardly alter the plane wave result.

4. (color online). The sensitivity of the pair correlation (PC) on the ω meson mass distribution spectrum. The solid and dashed curves describe respectively the calculated cross sections with and without PC incorporated in the nuclear density distribution (see text).

5. (color online). The effect of the detector resolution on the ω meson mass distribution spectrum. The solid curve corresponds to the cross section given in Eq. (15), where the detector resolution is not incorporated in the calculation. The dot-dashed curve represents the cross section where the detector resolution is incorporated in the calculation, see Eq. (20) in the text.

6. (color online). The calculated ω meson mass distribution spectra (solid curves due to Eq. (20)) in the $(\gamma, \omega \to \pi^0\gamma)$ reaction on ^{93}Nb nucleus for the ω meson momentum bins quoted in the figure. The histograms represent the measured $\pi^0\gamma$ invariant mass distribution spectra (taken from Ref. [25]), normalized to the calculated cross sections.

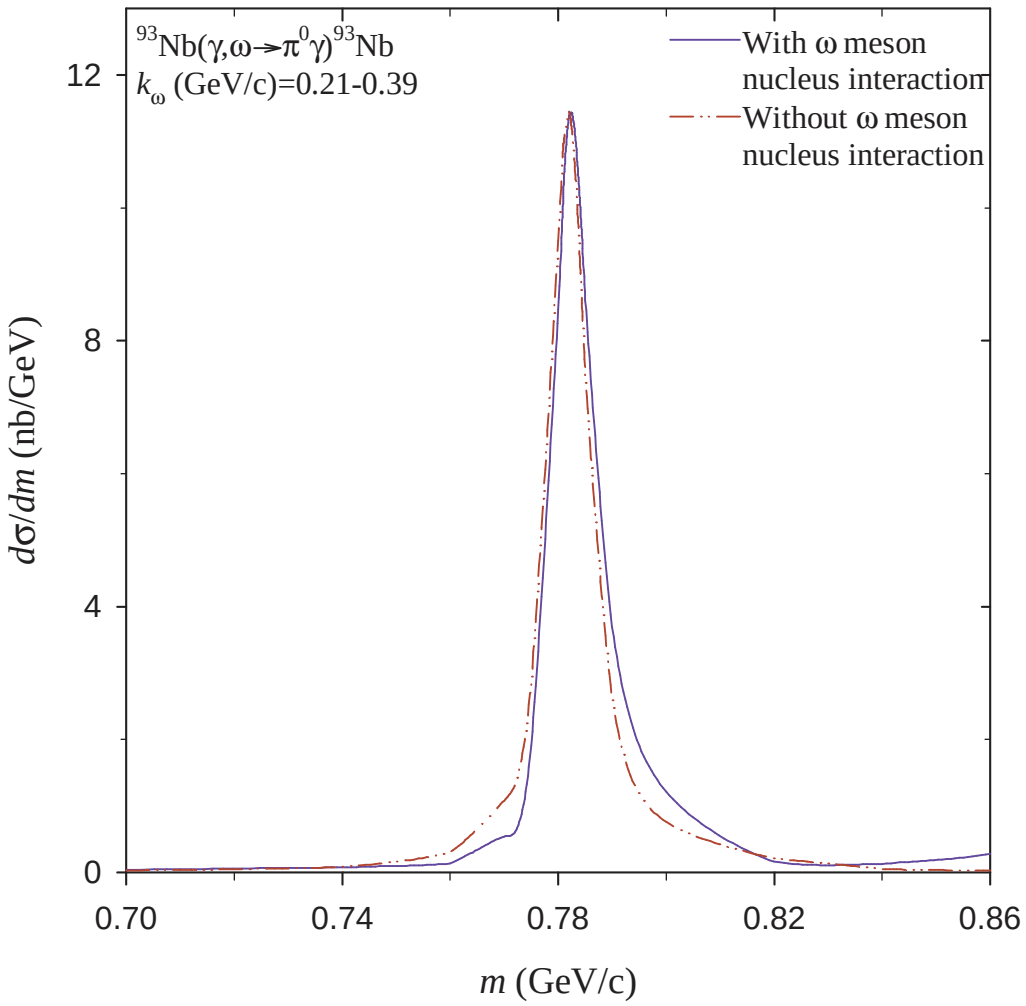
^{93}Nb(γ,ω→π^{0}γ)^{93}Nb
k_ω (GeV/c)=0.21-0.39
With ω meson nucleus interaction
Without ω meson nucleus interaction
dσ/dm (nb/GeV)
m (GeV/c)
0
4
8
12
0.70
0.74
0.78
0.82
0.86

Fig. 1

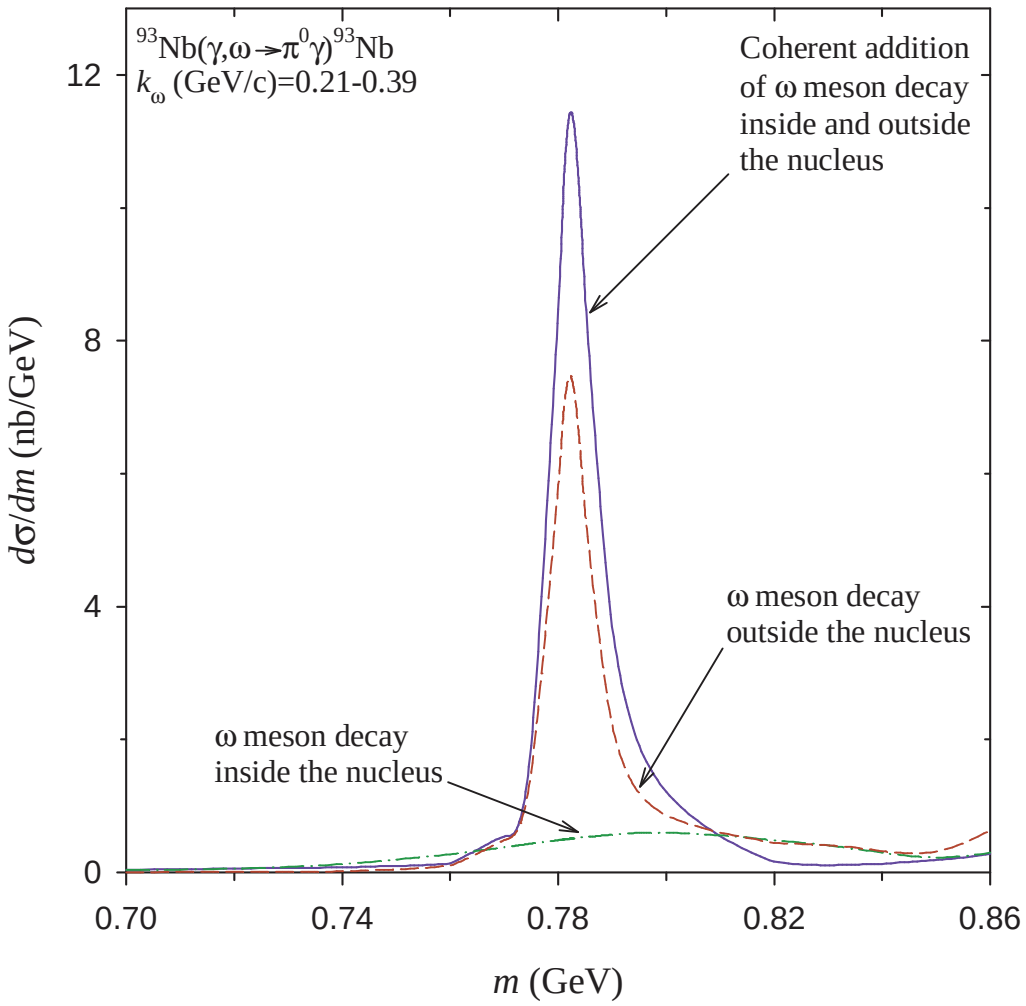
^{93}Nb(γ,ω→π^{0}γ)^{93}Nb
k_ω (GeV/c)=0.21-0.39
Coherent addition of ω meson decay inside and outside the nucleus
ω meson decay outside the nucleus
ω meson decay inside the nucleus
dσ/dm (nb/GeV)
m (GeV)
0
4
8
12
0.70
0.74
0.78
0.82
0.86

Fig. 2

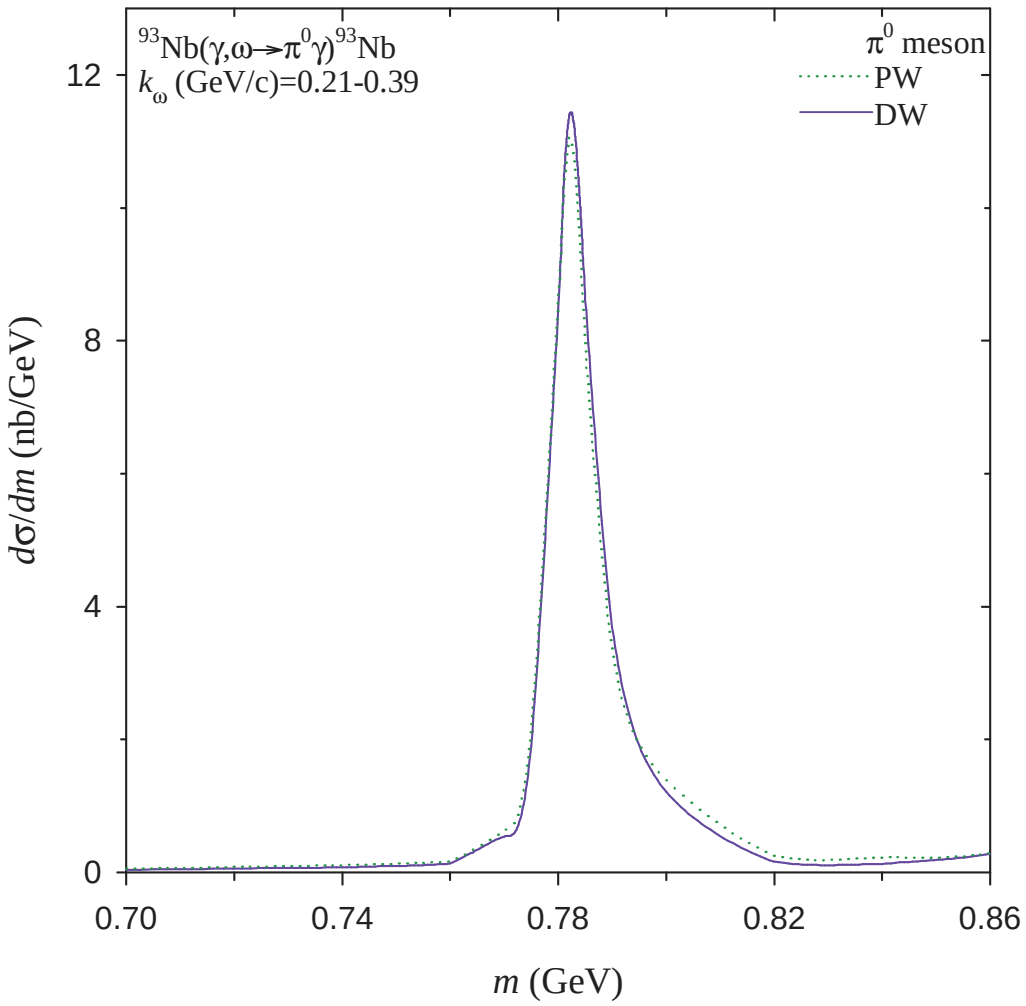
^{93}Nb(γ,ω→π^{0}γ)^{93}Nb
k_ω (GeV/c)=0.21-0.39
π^0 meson
PW
DW
12
8
4
0
0.70
0.74
0.78
0.82
0.86
$d\sigma/dm$ (nb/GeV)
m (GeV)

Fig. 3

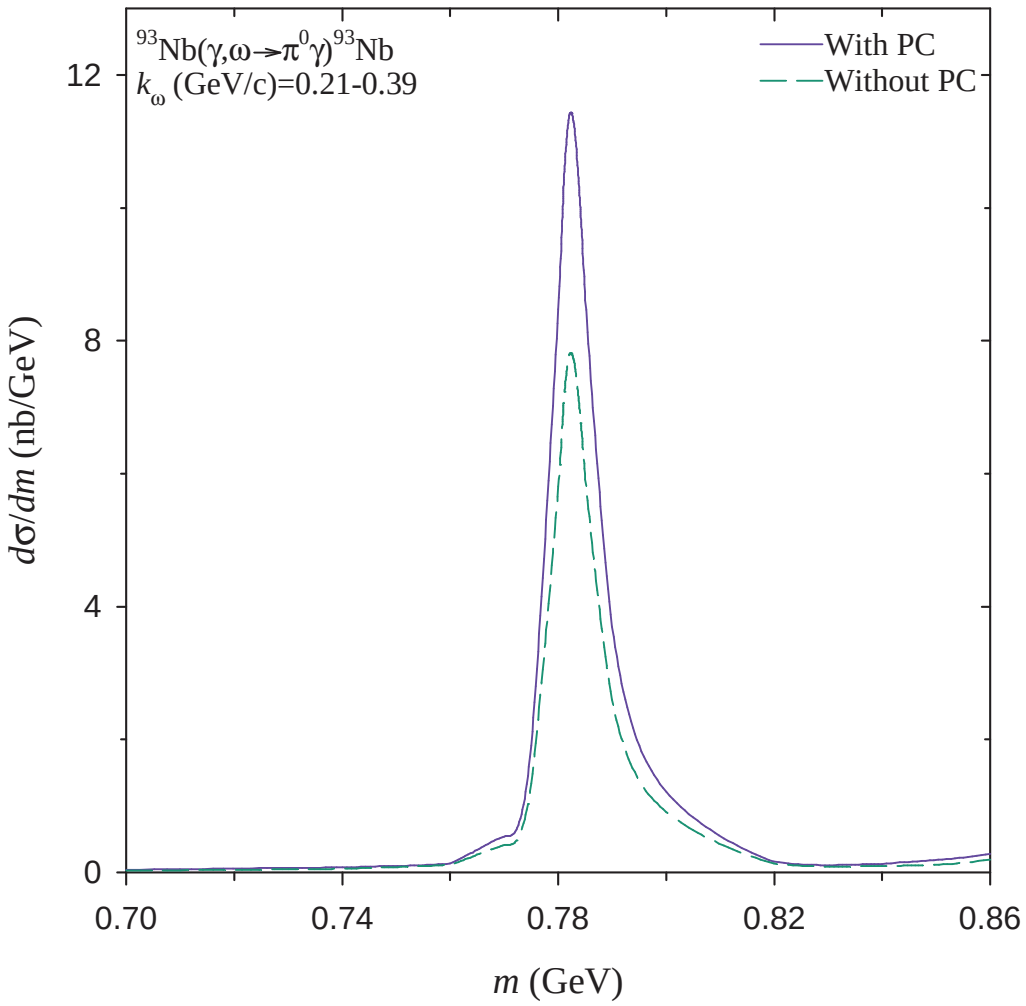
^{93}Nb(γ,ω→π^{0}γ)^{93}Nb
k_ω (GeV/c)=0.21-0.39
With PC
Without PC
12
8
4
0
0.70
0.74
0.78
0.82
0.86
dσ/dm (nb/GeV)
m (GeV)

Fig. 4

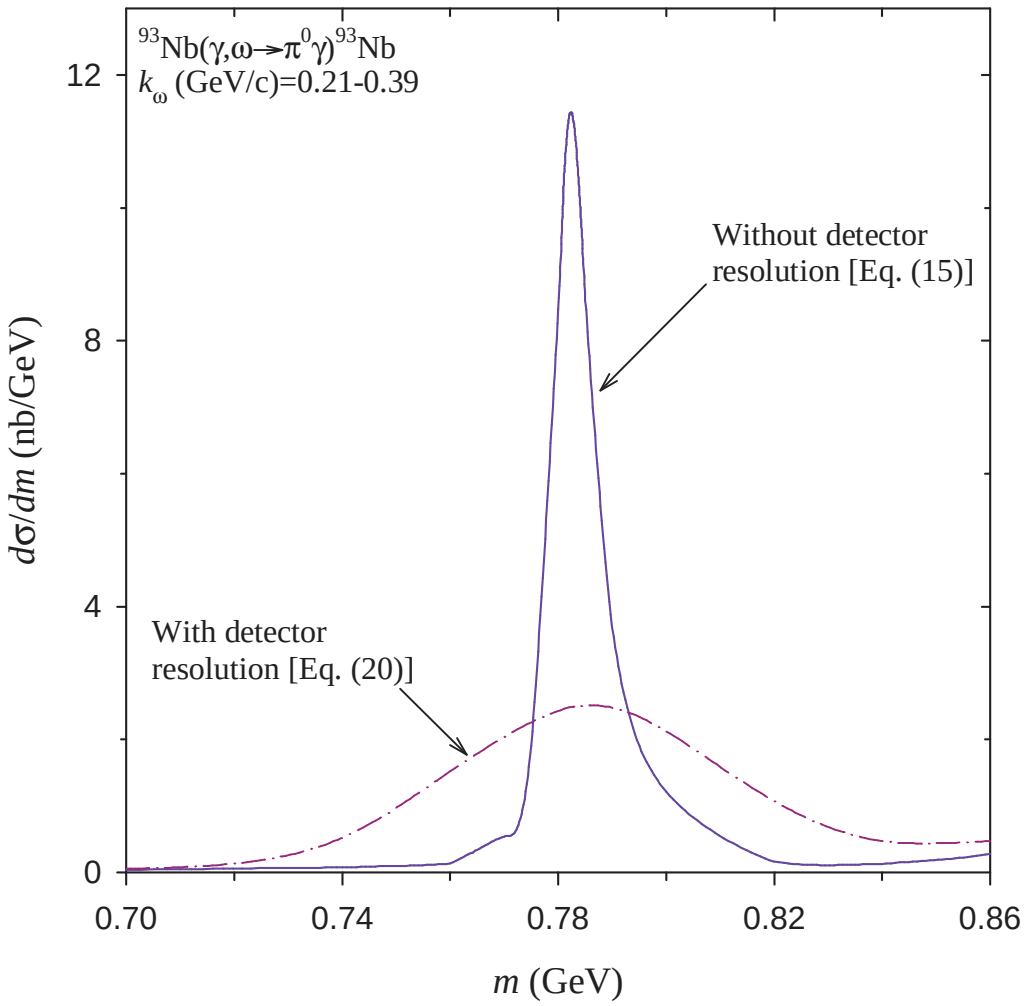
^{93}Nb(γ,ω→π^{0}γ)^{93}Nb
k_ω (GeV/c)=0.21-0.39
Without detector resolution [Eq. (15)]
With detector resolution [Eq. (20)]
dσ/dm (nb/GeV)
m (GeV)
0
4
8
12
0.70
0.74
0.78
0.82
0.86

Fig.5

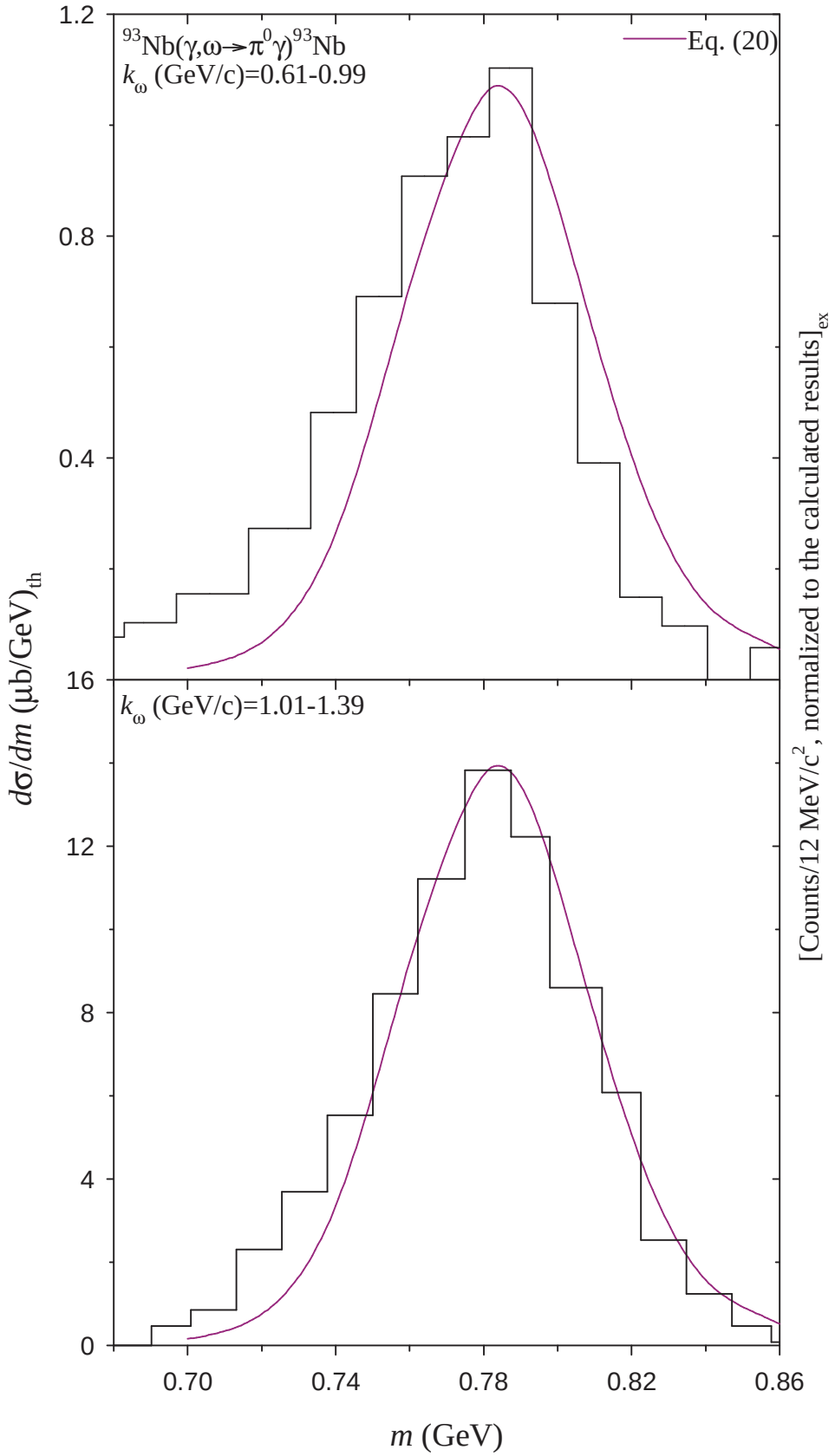
^{93}Nb(γ,ω→π^{0}γ)^{93}Nb
k_ω (GeV/c)=0.61-0.99
Eq. (20)
k_ω (GeV/c)=1.01-1.39
$d\sigma/dm$ (μb/GeV)$_{th}$
[Counts/12 MeV/c^2, normalized to the calculated results]$_{ex}$
m (GeV)
1.2
0.8
0.4
16
12
8
4
0
0.70
0.74
0.78
0.82
0.86

Fig.6